Adaptive Individual Blade Pitch Control of an Ocean Current Turbine for Load Reduction

Louis M. Lee & James H. VanZwieten, Department of Ocean and Mechanical Engineering, Florida Atlantic University

Key Words: ocean current energy, ocean current turbine, adaptive control, individual blade pitch control, load reduction, hydrokinetic power, marine renewable energy

Section 1: Introduction

Energy demand is constantly growing in our society. To help meet these demands, renewable resources including the energy available in the world oceans are being explored. Ocean current energy is a form of marine renewable energy that is accessible on the western boundaries of the world's oceans (VanZwieten et al 2013). On average, it has been estimated that about 19 GW of electrical power can be generated from ocean currents located off the east coast of the United States (Georgia Tech Research Corporation, 2013). The Florida Straits alone has an estimated 5.6 GW of theoretically extractable power (Yang et al 2013). This resource has an average kinetic energy flux that reaches 3.3 kW/m^2 in the Florida Straits (Machado et al 2016). According to the US National Renewable Energy Laboratory (2014), wind energy is broken down into seven wind power classes from class 1 to class 7. Utility scale wind turbines are considered suitable for areas designated as class 3, where mean power densities range from 0.15 to 0.20 kW/m^2 at a height of 10 m. The ocean current energy resource available in the Florida Straits provides more than 3 times the energy density of wind sites that are characterized as having a class 7 wind power resource, those providing an average of 1 kW/m^2 at a height of 10 m.

Ocean current turbines (OCT) are being designed to create electricity from these large scale ocean currents, with locations being considered for energy extraction including areas off: Florida (USA), North Carolina (USA), Japan, Taiwan, and South Africa. The OCT numerical model

used in this study represents a neutrally buoyant horizontal axis OCT design with a 20 m diameter rotor. This OCT is designed to operate in a mooring configuration where it is attached via a cable to a flounder plate that is connected to the main mooring line that runs from a surface buoy to the sea floor (Driscoll et al 2008) (see Figure 3). The numerical model of this OCT utilizes a blade element momentum rotor model with a dynamic wake inflow algorithm, algorithms that account for the hydrodynamic forces on the turbines main body, as well as the buoyancy compensation modules (VanZwieten et al 2013) (see Figure 2). More information about this OCT and artist renderings are available in (VanZwieten et al 2013) and (VanZwieten et al 2016).

Wind turbines, and likely future OCTs, typically operate in three distinct regions depending on the wind/current speeds and the rated power of the device. Region 1 is considered to be the startup region where the wind/current is just sufficient to turn the turbine on as defined in (Balas et al 2011). As the wind/current speed increases, the turbine is capable of producing electrical power that is less than the rated power. This operating condition can be referred to as Region 2 and is the region where controllers are developed primarily to maximize produced electrical power (Balas et al 2011). In Region 3, the current/wind speed is greater than what is required for rated power production (Balas et al 2011). Therefore, a turbine is typically operated at its rated speed and the blade pitch angles are manipulated so that the system operates at rated power. This study focuses on Region 2 operation, with minor changes required for implementing the presented algorithm in Region 3.

Due to varying current shear, the rotor blades on an OCT will experience a variation of current speeds throughout the revolution. As a result, cyclic loadings are encountered on the rotor blades when repeatedly passing through these positions. These periodic forces lead to fatigue damage of

the blades, possibly leading to blade failure (Frost et al 2009). Methods have been suggested to reduce the effect of the axial loads due to current shear by changing the pitch angle of the rotor blades as a function of rotation angle such that they experience nearly uniform forces as they rotate. Such methods require the implementation of an individual blade pitch (IBP) control technique, such as the one introduced by (Bossanyi 2003). This paper presents theory on an IBP controller that utilizes a Direct Adaptive Disturbance Rejection (DADR) approach (Section II). Sections III, IV, and V present the testing approach, results, and conclusions, respectively.

Section 2: Theory

Section 2.1: Background (Plant Parameters)

The selected DADR algorithm is developed based on a linear, time-invariant, and finite dimensional plant model, as defined by (Balas et al 2011), that comes in the form of a state and output equation represented in its generic form as:

$$\begin{cases} \dot{x_p} = Ax_p + Bu_p + \Gamma u_D \\ y_p = Cx_p; x_p(0) = x_0 \end{cases}, \quad (1)$$

where x_p is the plant state vector, u_p is the control input vector, y_p is the sensor output vector, u_D is the input disturbance vector that is assumed to come from the disturbance generator, A represents the state matrix, B represents the input matrix, Γ represents the disturbance matrix, and C serves as the output matrix. For the application of this study, the simulation uses a fully non-linear model with 14 system states including three-position, three-attitude, three-linear velocity, rotor rpm, and rotor rotation angle with control inputs and outputs discussed later in sub-sections 2.2 and 3.2.

Section 2.2: Control Algorithm

The purpose of this IBP controller is to cyclically adjust (as a function of rotor rotation angle) the blade pitch such that the variation in the axial bending moments on these blades are minimized throughout a revolution. To start this DADR process, it is important to first select basis functions that relate the adaptive gains to a control solution that can reduce the disturbance (Landau et al 2011). The selected basis functions and associated control law used for calculating the individual blade pitch angles were presented by (Balas et al 2011) and has the following form:

$$u_p = G_D \varphi_D, \quad (2)$$

where u_p is the output from the control algorithm that is fed back into the plant as an input, G_D is the adaptive gain matrix, and φ_D are the basis functions used for the three bladed rotor. This form is used because it is based on an easily measurable system state of the bladed rotation angle which is directly linked to the shear force disturbance. Equation (2) can be better visualized for a three bladed rotor in its expanded form:

$$[u_3\ u_2\ u_1] = [G_1 \quad G_2] \begin{bmatrix} \sin(\theta) & \sin\left(\theta + \frac{2\pi}{3}\right) & \sin\left(\theta + \frac{4\pi}{3}\right) \\ \cos(\theta) & \cos\left(\theta + \frac{2\pi}{3}\right) & \cos\left(\theta + \frac{4\pi}{3}\right) \end{bmatrix}, \quad (3)$$

where u_1, u_2, and u_3 are the individual blade root pitch angles in radians specified by the controller with u_1 representing the pitch angle of the leading blade positioned $4\pi/3$ radians ahead of the third blade; G_1 and G_2 are the adaptive gains in radians; and the last terms are the basis functions written in their expanded form. On OCTs and wind turbines, the root pitch angles are the actuated components. By actuating the root angle, the angle of attack along the entire blade is changed.

In order to adaptively calculate the gains associated with this control law, the axial bending moment at the root of these blades and the rotor azimuth angle are used as inputs to an adaptive

controller. The azimuth angle is calculated using the position of the leading blade with respect to the vertical position, as illustrated in Figure 1.

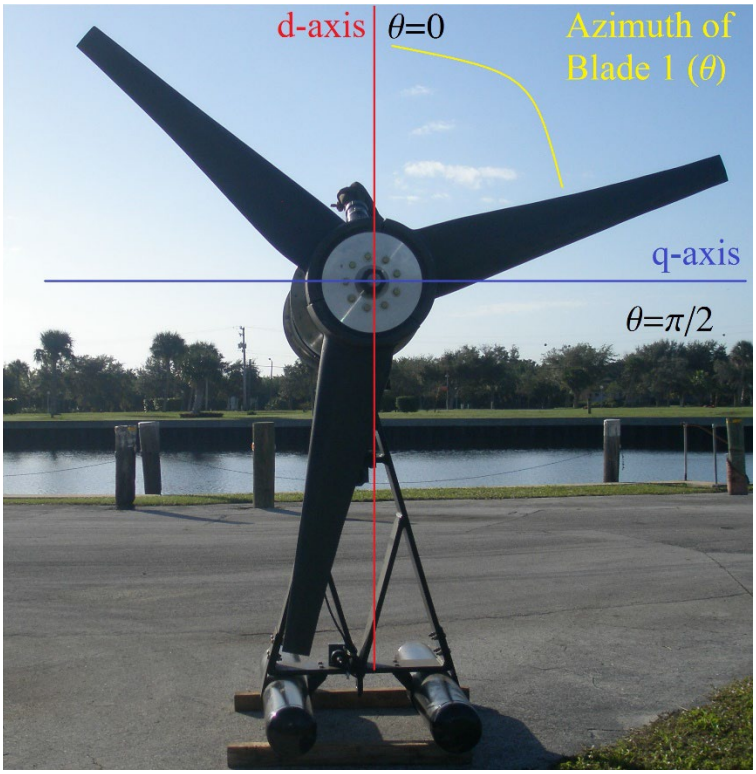

Figure 1: Presents the azimuth angle (θ) and the direct and quadrature axes used to model the OCT.

The gains used in this controller are tuned using the adaptive gain law introduced by (Balas et al 2011):

$$\dot{G_D} = -e_y \varphi_D^T \gamma_D, \qquad (4)$$

where γ_D is an arbitrary positive scalar that can be tuned to modify the convergence rate of the adaptive controller gains. A stability analysis has proven that this adaptive controller and adaptive gain law are stable when the plant characterized by equation (1) is almost strictly

positive real (ASPR) with positive high frequency gain and the plant is minimum phase (Balas et al 2011).

This adaptive gain law above can also be written as:

$$\dot{G}_D = -\begin{bmatrix} M_d \\ M_q \end{bmatrix} \gamma_D. \qquad (5)$$

These measured inputs are in the direct and quadrature (d-q) perpendicular axis borrowed from the three phase electrical machine theory. These are calculated from the three root bending moment signals that were transformed into a mean value and variations about two orthogonal axes as explained by (Bossanyi 2003), with the d-axis oriented vertically upward ($\theta = 0$) and the q-axis oriented horizontally ($\theta = \frac{\pi}{2}$) as shown in Figure 1. This controller requires 4 measured inputs: the azimuth angle (θ) and three bending moments (M_1, M_2, and M_3), also referred to as the output tracking error, which are the measured axial bending moments of blades 1, 2, and 3 respectively. These inputs are used in the following equation (Bossanyi 2003) to calculate the bending moments in the d-q axis,

$$\begin{bmatrix} M_d \\ M_q \end{bmatrix} = \frac{2}{3}\begin{bmatrix} \cos(\theta) & \cos(\theta + \frac{2\pi}{3}) & \cos(\theta + \frac{4\pi}{3}) \\ \sin(\theta) & \sin(\theta + \frac{2\pi}{3}) & \sin(\theta + \frac{4\pi}{3}) \end{bmatrix}\begin{bmatrix} M_3 \\ M_2 \\ M_1 \end{bmatrix}. \qquad (6)$$

These blades will sequentially rotate through a fixed azimuth angle in the following order: blade 1, blade 2, and then blade 3, with blade 1 being $4\pi/3$ radians ahead of the last blade as discussed earlier in this section. The M_d and M_q terms are the axial bending moments in the direct and quadrature axes.

Equation 4 can now be written in the expanded form by combining Equations 5 and 6 to yield:

$$\begin{bmatrix}\dot{G}_1\\ \dot{G}_2\end{bmatrix} = -\left[\frac{2}{3}\begin{bmatrix}\cos(\theta) & \cos\left(\theta+\frac{2\pi}{3}\right) & \cos\left(\theta+\frac{4\pi}{3}\right)\\ \sin(\theta) & \sin\left(\theta+\frac{2\pi}{3}\right) & \sin\left(\theta+\frac{4\pi}{3}\right)\end{bmatrix}\begin{bmatrix}M_3\\ M_2\\ M_1\end{bmatrix}\right]\gamma_D. \qquad (7)$$

In summary, when the rotor blades experience a harmonic change in bending moment at the root due to current shear during rotation, the controller adapts the controller gains that are multiplied by the basis functions to drive the differential moment towards 0. The DADR approach has also been previously used to reduce the cyclic loading on high-fidelity wind turbine models (Magar et al 2015).

Section 3: Testing Approach

Section 3.1: Ocean Current Turbine Model and Design

The OCT that is numerically modeled is based on a neutrally buoyant ocean current turbine design created by the Southeast National Marine Renewable Energy Center (SNMREC) at Florida Atlantic University (FAU) as presented by (Driscoll et al 2008). This horizontal axis OCT was initially designed with a rated power of 20 kW and a three bladed rotor which spans 3 m in diameter. Buoyancy compensation modules are used in this design to create neutral buoyancy and a counteracting force for the hydrodynamic torque of the rotor (see Figure 2). The OCT was designed to be operated in a single-point mooring system in the Gulf Stream. The mooring system consists of a mooring buoy to be deployed on site, as well as a support platform or vessel to be towed to the operational site while carrying the OCT. The OCT will then be connected to the mooring buoy and anchor via a flounder plate and deployed for operation (see Figure 3). The system simulated in this paper is based on this design, but has a 20 m rotor blade that is designed for variable blade pitch operation (VanZwieten et al 2016). In addition, this OCT

system uses length, area, volume, and inertial properties that are scaled from those in (Driscoll et al 2008) by 20/3, $(20/3)^2$, $(20/3)^3$, and $(20/3)^5$ respectively.

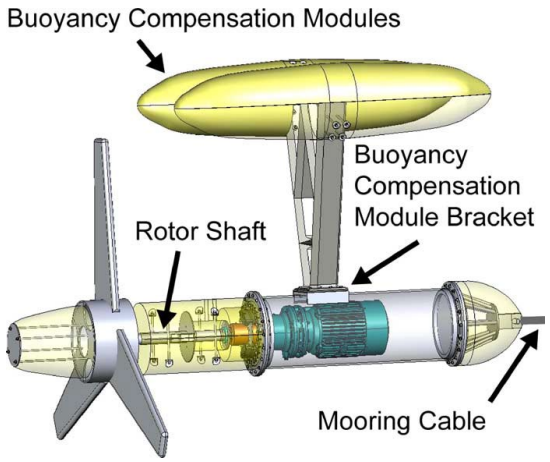

Figure 2: Shows the OCT design and primary components

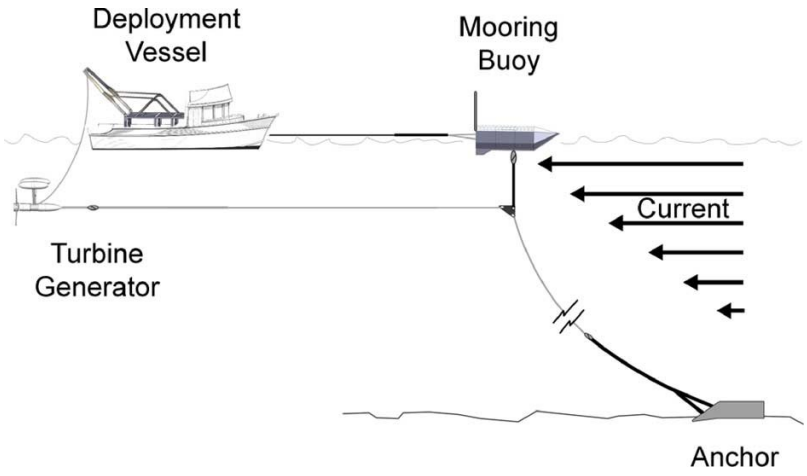

Figure 3: Shows the OCT deployed in the single-point mooring configuration.

Section 3.2: Numerical Modeling

The numerical simulation uses a physics based nonlinear mathematical model developed using Simulink and MATLAB of the OCT design described in Section 3.1. This model was developed primarily for the analysis of system dynamics and development of control systems. The utilized

numerical simulation approach is described by (VanZwieten et al 2013) with the modifications for simulating the described system with variable pitch rotors described by (VanZwieten et al 2016). This mathematical model is used to create a 7-DOF dynamics simulation (standard 6-DOF for a rigid body and the relative rotor blade rotation with respect to this rigid body) of the OCT which calculates the NED position, Euler angles, linear and angular velocities, and the axial rotation angle and angular velocity of the rotor. The simulation also implements a finite element lumped mass model (Radanovic and Driscoll 2012) of the cable that attaches the OCT to the connecting mooring line, an unsteady blade element momentum (BEM) rotor model, models of the hydrodynamic forces on the body of the OCT, and the buoyancy compensation modules (VanZwieten et al 2013).

Section 3.3: Simulation Operating Parameters

The numerical simulation implements specified operating parameters of the OCT based on previously measured data conducted by the SNMREC. OCT's operating in the Gulf Stream will be affected by ocean currents that vary both temporally and spatially. Site specific water velocity measurements were collected to define the range of water velocities that the OCT would likely operate in, as well as vertical water velocity gradients that are potentially encountered. In (VanZwieten et al 2013), ocean current measurements taken off southeast Florida (26°04.3' N, 79°50.5' W) over a 13-month period from February 2009 to March 2010 were summarized (see Figure 3). Additional measurements recorded from 2001 and 2002 over a 19-month period at 26°11' N, 79°50' W are presented in (Raye et al 2002). Both sets of data yielded a mean near surface current speed of 1.6 m/s (see Figure 4). The data used in (VanZwieten et al 2013) were also used to calculate the mean vertical current shear of 0.004 (m/s)/m with only minimal data

points exceeding 0.03 (m/s)/m as shown below (see Figure 5). These are the respective mean and maximum current shear values that are used for the numerical simulations.

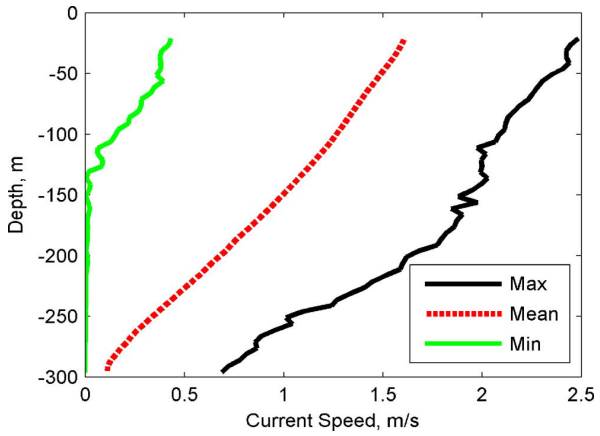

Figure 4: Maximum, mean, and minimum current velocities measured using a 75-kHz acoustic Doppler current profiler (ADCP) offshore Ft. Lauderdale, FL from February 2009 to March 2010.

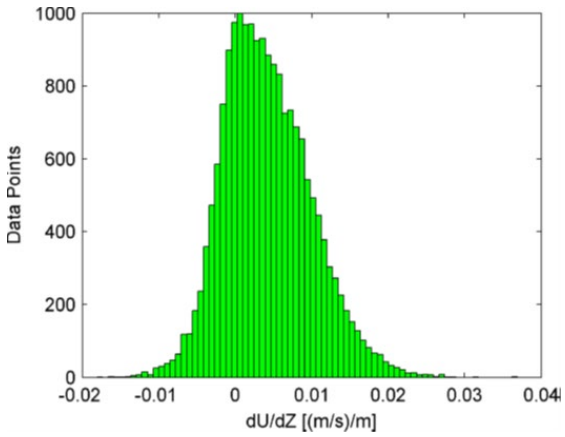

Figure 5: Vertical current gradient at a depth of 40 m measured using a 75-kHz ADCP offshore Ft. Lauderdale, FL from February 2009 to March 2010.

All simulations are run with a turbine hub depth of 30 m to maintain the mean current speed at the hub to mimic similar operating conditions for the OCT operating offshore Ft. Lauderdale as presented in Figures 4 and 5. The two operating conditions evaluated include both the mean and

maximum current shears presented in (VanZwieten et al 2013). In order to maintain the mean current velocity of 1.6 m/s at the hub depth of 30 m, a surface current speed of 1.72 m/s was used for simulations where the OCT operated in the mean current shear of 0.004 (m/s)/m. Likewise, to maintain the mean current speed of 1.6 m/s at hub depth for the simulations operating in the maximum current shear of 0.03 (m/s)/m, a surface current speed of 2.5 m/s was used.

Section 3.4: Numerical Simulations

For each operating condition the numerical simulation is run using two different approaches. First, the main body of the OCT system is held stationary within the water column and the rotor is allowed to rotate. This is done to more clearly analyze the impact of current shear on the performance of the OCT without the couple effects from the single-point mooring system. The second analysis includes mooring system effects into the simulation. The simulation with the moored configuration allows for observation and analysis of the OCT under more realistic operating dynamics for a moored system operating offshore Ft. Lauderdale. For both operating configurations, simulations are run separately for the mean and maximum current shear values.

As the current flows through the turbine, the blades immediately experience axial bending moments at the root. These bending moments can range in the magnitude of up to Mega-Newtons (10^6 Newtons) and cause fatigue on the rotor blades due to the cyclic loading. These and other forces can continuously alter the stress distribution on the blades impacting the operation life of the blades (Akram 2010). When operating in a current shear, the bending moments experienced by the blades become nearly harmonic. When operating in a vertical shear, a rotor blade passing through the vertically upwards orientation will have forces that can be approximated as the crest of the sine wave with the lowest position oriented vertically downwards corresponding to the trough. The objective of the numerical simulations are first, to

model and analyze the cyclic axial forces acting on the OCT's rotor blades during operations in various conditions and second, to reduce the cyclic forces acting on the blade by implementation of the adaptive controller.

Section 4: Results

All simulations were run for a total time of 330 seconds. The simulation assumes that the OCT is placed directly into the specified current at the beginning of the simulation and therefore, a transient condition is observed in each simulation that lasts for about 30 seconds. To analyze the effects of the adaptive controller after the OCT has achieved a state of equilibrium, a 30 second time delay has been implemented before the adaptive controller turns on. These first 30 seconds are not presented in the figures and not included when calculating the presented statistics.

Section 4.1: Simulation Results for a Stationary System in Mean Current Shear

In order to observe the response characteristics of the adaptive controller, the OCT was simulated in a stationary configuration (with no mooring) with the mean current (of 1.72 m/s at sea surface) and mean current shear (of 0.004 (m/s)/m). This allowed for analysis of the axial bending moments experienced by the rotor blades and the effect of the adaptive controller. Figures 6, 7, and 8 show the calculated rotor blade axial bending moments as a function of time.

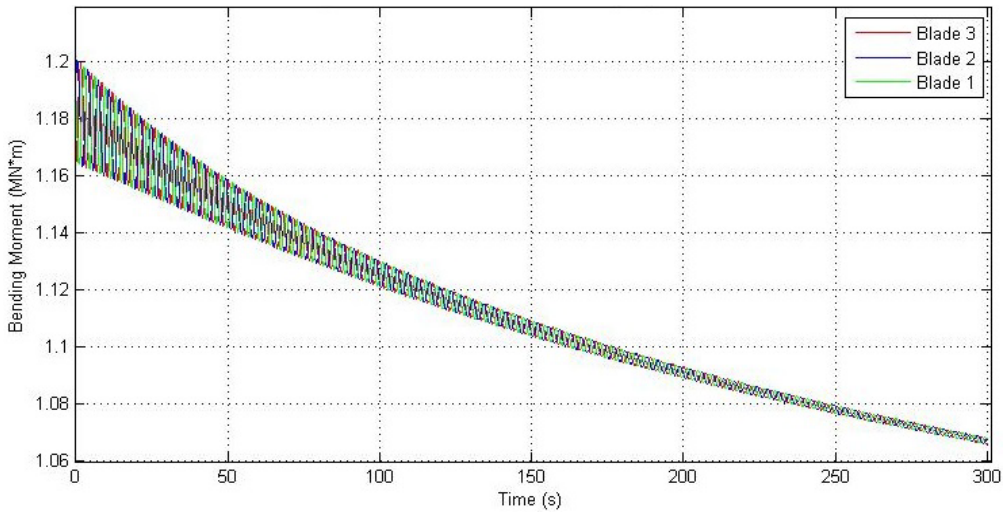

Figure 6: Harmonic oscillations of the 3 blades in the stationary configuration and the reduction in loads over 300 seconds.

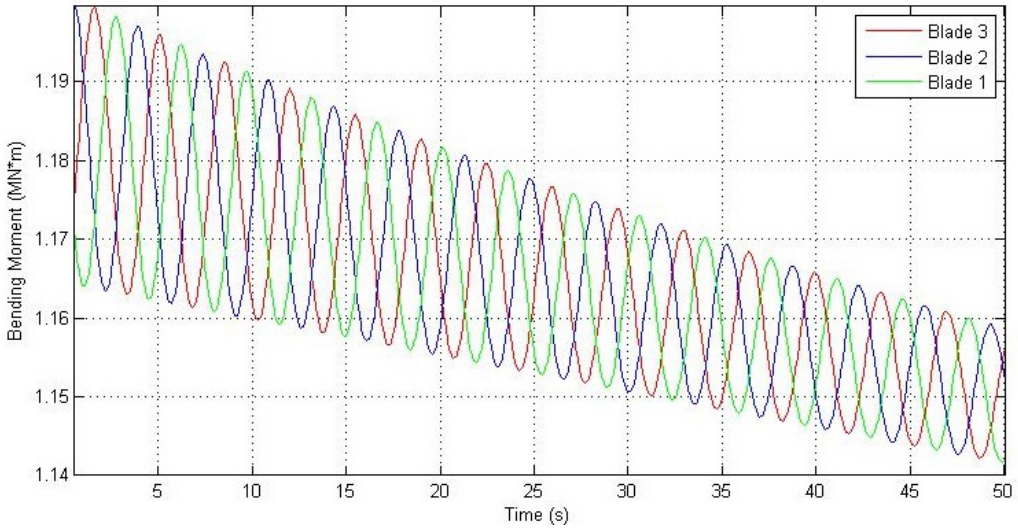

Figure 7: First 50 seconds of the harmonic oscillations in the stationary configuration to show detail.

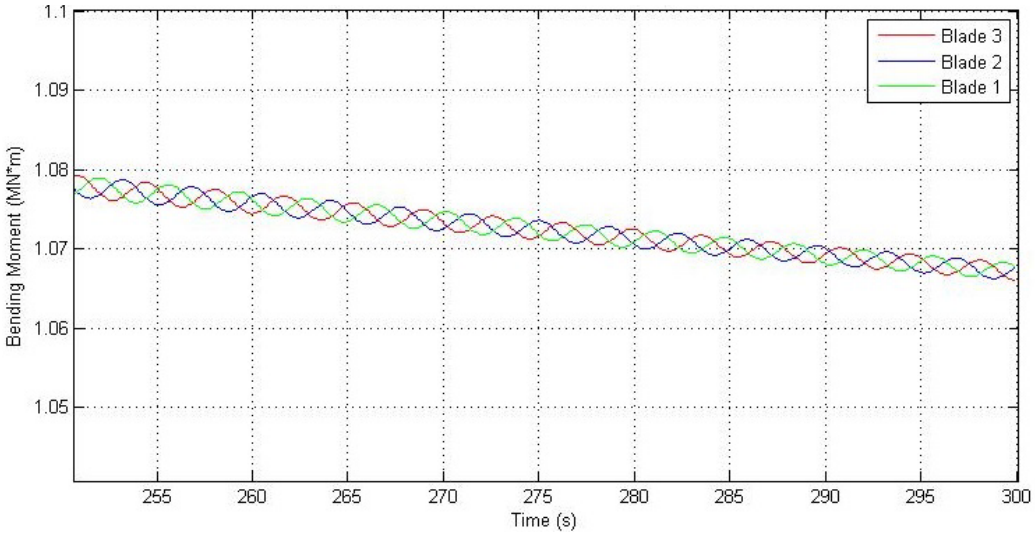

Figure 8: Last 50 seconds of the harmonic oscillations in the stationary configuration to show detail.

As stated in section 3.4, the axial loads on the rotor blades show harmonic oscillations that vary as the blades rotate about the rotor shaft. All three blades initially experience bending moment variations of 34 kN-m (see Figure 7). These initial oscillations are at a time when the adaptive gains are just beginning to be tuned from their initial values of 0, and therefore essentially represent the case where no IBP control is utilized. At the end of the five minute simulation the magnitude of the bending moment oscillations have been reduced to 3 kN-m (Figure 8). This shows that in only 5 minutes the adaptive controller has reduced the moment amplitude by 91.18% which represents a significant improvement over not utilizing IBP control. The bending moments of the blades will also continue to steadily converge to a lower limit over time. The low frequency convergence from approximately 1.18 MN-m to 1.07 MN-m is also due to the root twist of the rotor blades. All three blades show evidence of the same load reduction due to the adaptive controller (see Figure 6).

The convergence of the adaptive gain values of the stationary system with a current shear of 0.004 (m/s)/m are presented below (see Figure 9). After the simulation was run, the value of G_1 converged to a value of 0.139 radians (7.96°). The value of G_2, which is the gain for the mean moment in the horizontal direction, remained at approximately 0. This is the optimal value because the secondary effects caused by the tangential induction of the oncoming flow are small when both the turbine and current shear are vertical. This result induces a control signal where the amplitude of the sinusoidal blade root pitch variation is 7.96° for each full rotation of the blades under these operating conditions.

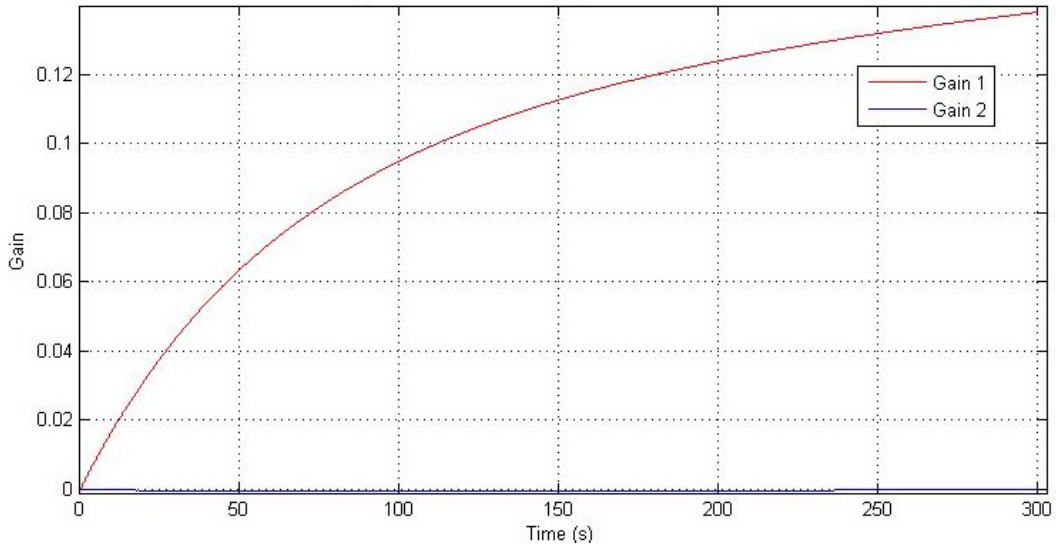

Figure 9: Plot showing the adaptive gain convergence of the stationary system.

In order to observe the performance of the adaptive controller under realistic operating conditions, the OCT was simulated to operate in the moored configuration with a mean current shear (with a current shear of 0.004 (m/s)/m and a surface current speed of 1.72 m/s). This allowed for the analysis of the OCT being moored off the coast of Ft. Lauderdale and the effects of the adaptive controller under these operating conditions. Figures 10, 11, and 12 show the simulation results in the form of the rotor blade axial bending moments plotted over time.

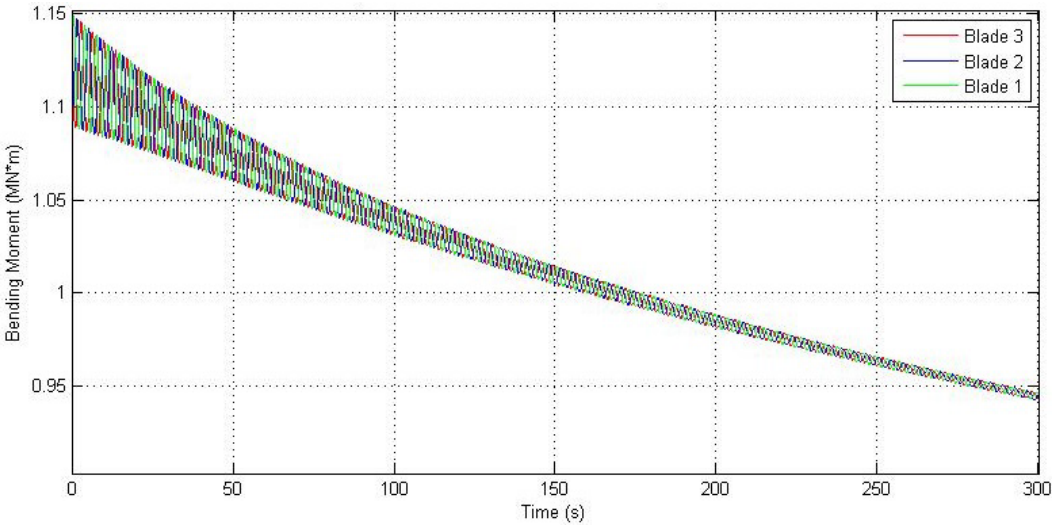

Figure 10: Harmonic oscillations of the 3 blades in the moored configuration and the reduction in loads over 300 seconds.

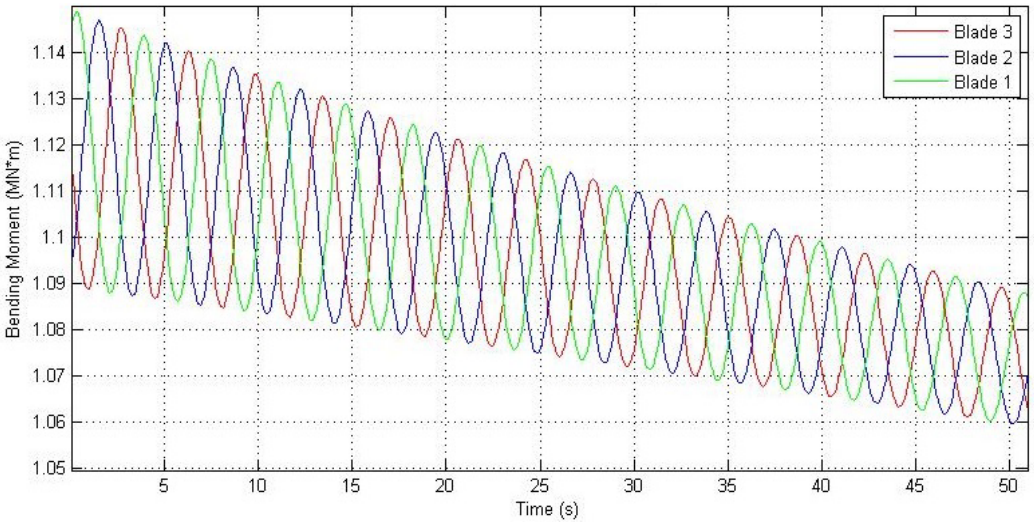

Figure 11: First 50 seconds of the harmonic oscillations in the moored configuration to show detail.

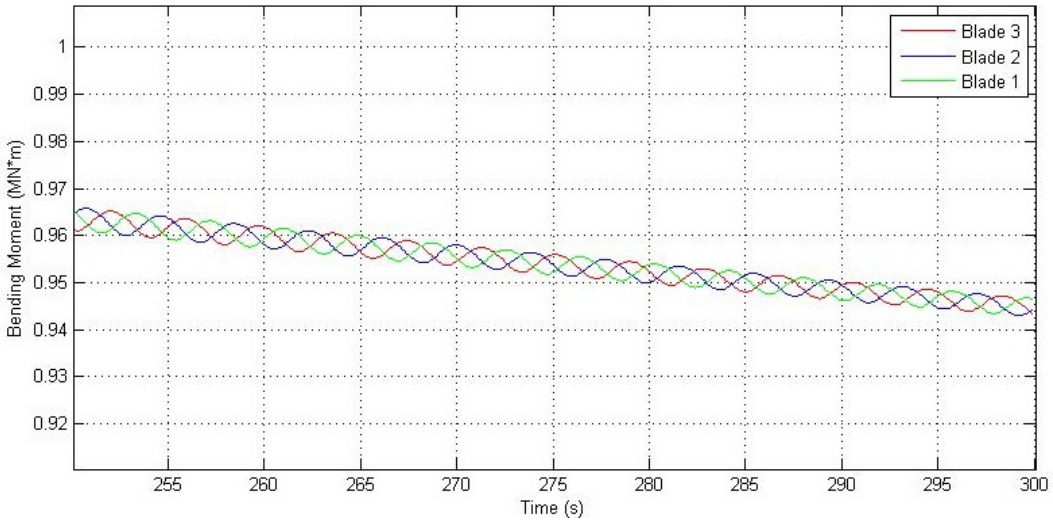

Figure 12: Last 50 seconds of the harmonic oscillations in the moored configuration to show detail.

Here, all three blades initially experience bending moment variations of 61 kN-m (see Figure 11). At the end of the five minute simulation, all three blades experienced moment variations of 4.7 kN-m (see Figure 12). The IBP controller reduced the moment amplitude by 92.3% over the course of five minutes. The initial moment variation in the moored configuration is greater than that of the stationary configuration by 44.3%, primarily caused by a misalignment between the rotor axis and the flow. After the five minute simulation, the moment variation in the moored simulation is greater than that of the stationary configuration by 36.2%. The OCT simulated in the moored configuration showed that the rotor blades experienced initial axial blade loads smaller in magnitude than that of the stationary configuration by 4.09% and by 11.3% after five minutes of controller tuning.

The convergence of the adaptive gain values when applied to the moored system with the mean current shear are presented in Figure 13. The effects of the mooring system impacted the gain convergence. The value of G_1 reached a value of 0.228 radians after the OCT was operated for

five minutes and G_2 reached a value of 0.058 radians at the end of the simulation. This gain is no longer approximately zero since the mooring system changed the alignment of the turbine with the flow producing additional cyclic loadings beyond those caused by current shear. Additionally, a relative rotor rotation angle of 0 degrees is no longer vertical since the system has a roll angle that was induced by the rotor torque. The ability of this controller to directly adapt to these loading changes is one of the benefits to using this controls approach. Fixed gain approaches based on model performance estimates will likely not be able to efficiently predict coupled effects such as these.

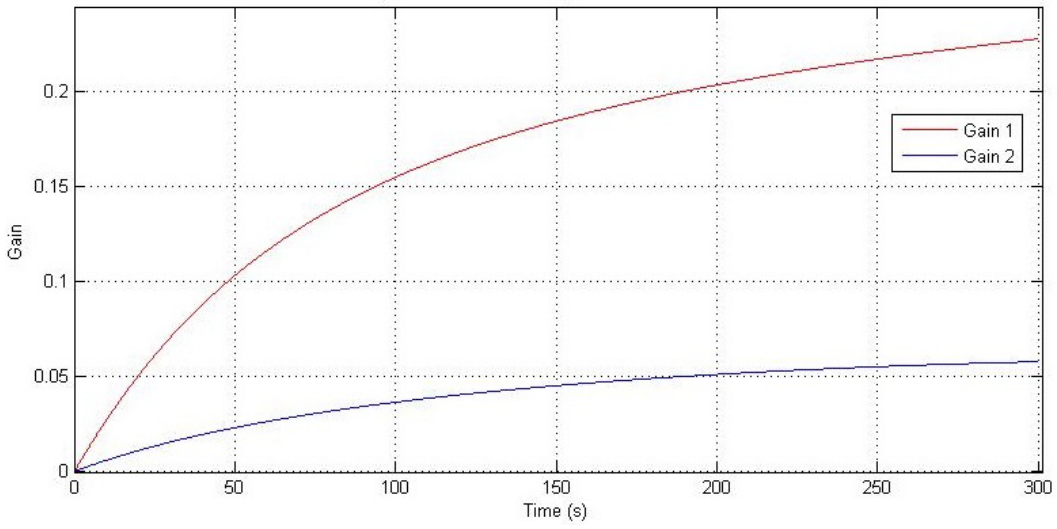

Figure 13: Shows the adaptive gains of the moored system after 300 seconds.

Simulations were also run using the maximum measured current shear value in the Gulf Stream of 0.03 (m/s)/m presented by (VanZwieten et al 2013), with the stationary and moored configurations. The simulation from the stationary configuration initially revealed that all three blades experienced varying moments of 272 kN-m and varying moments of 16 kN-m at the end of the simulation. The moored simulation revealed initial varying moments of 255 kN-m with the oscillations reduced to 46 kN-m. This revealed a 94.12% and 81.88% reduction in moment

amplitude for the stationary and moored simulations, respectively. The adaptive gain values of G_1 and G_2 were 1.031 and 0 radians for the stationary simulation and 1.415 and 0.1297 radians for the moored simulation, respectively. Greater moment amplitude reduction was observed for the stationary configuration when simulated with the maximum current shear.

Section 5: Conclusion

A direct adaptive disturbance rejection control algorithm has been shown through numerical simulation testing to significantly reduce the cyclic axial loadings on an ocean current turbine's rotor blades. The numerical model was set to represent an OCT operating in both stationary and moored configurations where the mean current shear is 0.004(m/s)/m, surface current speed is 1.72 m/s, and operating depth is 30 m to represent mean operating conditions off the coast of Ft. Lauderdale. The OCT simulated in the stationary configuration showed the adaptive controller reduced the moment amplitude of the harmonic oscillations by 91.18%. The adaptive controller operated in the moored configuration reduced the moment amplitude of the axial bending moments experienced by the rotor blades by 92.3%. This suggests that the adaptive controller performed well in both cases. The simulations with a maximum current shear value of 0.03 (m/s)/m with surface current speed of 2.5 m/s revealed that the adaptive controller performed better with a greater moment amplitude reduction of 94.12% in the stationary configuration than the 81.88% reduction observed from the moored configuration.

Acknowledgements

The authors would like to thank the FAU's Office of Undergraduate Research and Inquiry for supporting this work through their Summer Undergraduate Research Fellowship program. The authors would also like to thank Parakram Pyakurel for contributing to this paper with his participation funded by the National Science Foundation (NSF) and specifically the Energy, Power, Control and Networks (EPCN) program within the framework of grant ECCS-1307889 'Collaborative Research: Optimized Harvesting of Hydrokinetic Power by Ocean Current Turbine Farms Using Integrated Control'. SNMREC is supported by the U.S. Department of Energy and the State of Florida.

Works Cited

Georgia Tech Research Corp., "Assessment of energy production potential from ocean currents along the United States coastline," Georgia Tech Research Corp., Atlanta, GA, 2013, Accessed: January 22, 2015. Available: http://energy.gov/sites/prod/files/2013/12/f5/energy_production_ocean_currents_us_0.pdf

J. H. VanZwieten Jr., A.E.S. Duerr, G.M. Alsenas, & H.P. Hanson, "Global ocean current energy assessment: an initial look," in Proceedings of the 1st Marine Energy Technology Symposium (METS13) hosted by the 6th annual Global Marine Renewable Energy Conference, April 10-11, Washington D.C, 2013. Available: http://www.foroceanenergy.org/mets/2013-peer-reviewed-mets-papers/

X. Yang, K.H. Haas, & H.M. Fritz, "Theoretical assessment of ocean current energy potential for the gulf stream system," Marine Technology Society Journal, 47(4), 2013, 101–112.

J. H. VanZwieten, N. Vanrietvelde, and B. Hacker, "Numerical simulation of an experimental ocean current turbine" Journal of Oceanic Engineering, 38 (1), 2013, 131-143.

E. A. Bossanyi, Individual blade pitch control for load reduction. Wind Energy 6, 2013, 119–128.

M. J. Balas, K. T. Magar, Q. Li, "Adaptive Disturbance Tracking Control for Large Horizontal Axis Wind Turbines with Disturbance Estimator in Region II Operation," AIAA 49th Aerospace Sciences Meeting including the New Horizons Forum and Aerospace Exposition, 2011.

S. A. Frost, M. J. Balas, and A. Wright, "Adaptive Control of a Utility -Scale Wind Turbine Operating in Region III". In Proceedings of 47th AIAA Aerospace Science Meeting Including the New Horizons Forum and Aerospace Exposition, 2009.

K. T. Magar, M. J. Balas, S. Frost, "Direct Adaptive Control for Individual Blade Pitch Control of Wind Turbines for Load Reduction," Journal of Intelligent Material Systems and Structures, 2015.

R. E. Raye, "Characterization study of the Florida Current at 26.11 north latitude, 79.50 west longitude for ocean current power generation," M.S. thesis, Dept. Ocean Eng., Florida Atlantic Univ., Boca Raton, FL, 2002.

I. D. Landau, R. Lozano, M. Saad, A. Karimi, "Adaptive Control: Algorithms, Analysis and Applications," 2nd Edition. Springer-Verlag London, 2011, 590 p. Hardcover ISBN: 978-0-85729-663-4.

National Renewable Energy Laboratory. (2014 February 6). *Dynamic Maps, GIS Data, and Analysis Tools: Wind Data Details* [Online]. Available: http://www.nrel.gov/gis/wind_detail.html

F. R. Driscoll, G. M. Alsenas, P. P. Beaujean, S. Ravenna, J. Raveling, E. Busold, C. Slezycki, A 20 kW open ocean current test turbine, in: MTS/IEEE Oceans Conference, Quebec City, Canada, September 15–18, 2008, No. OCEANS.2008.5152104.

J. VanZwieten, F. R. Driscoll, A. Leonessa, and G. Deane, "Design of a prototype ocean current turbine—Part II: Flight control system," Ocean Eng., vol. 33, pp. 1522–1551, Aug. 2006.

M. C. P. M. Machado, J. H. VanZwieten, and I. Pinos, "A Measurement-Based Analysis of the Hydrokinetic Energy in the Gulf Stream," Journal of Ocean and Wind Energy, vol. 3, no. 1, pp. 25-30, Feb. 2016.

M. W. Akram, "Fatigue Modeling of Composite Ocean Current Turbine Blade," M.S. thesis, Dept. of Ocean and Mech. Eng., Florida Atlantic Univ., Boca Raton, FL, 2010.

J. H. VanZwieten, P. Pyakurel, T. Ngo, C. Sultan, N. I. Xiros, "An assessment of using variable blade pitch for moored ocean current turbine flight control" International Journal of Marine Energy, 13, 2016, 16-26

B. Radanovic and F. R. Driscoll, "Development of an efficient general purpose cable model and simulation for marine application", Proceedings of the MTS/IEEE Oceans Conference, October 29-31, 2012, pp. 2060-2067